 Microsc. Microanal. 25 (Suppl 2), 2019
doi:10.1017/S143192761901239X

STEM Characterization of Metal Dusting Corrosion in Ni-based Alloy 600 and Fe-based Alloy 800H Exposed to a High Pressure Environment

Wei-Ting Chen[1,2,*], Bingtao Li[1], Mathias Galetz[3], and Brian Gleeson[1]

1. Department of Mechanical Engineering and Materials Science, University of Pittsburgh, Pittsburgh, PA, USA
2. Materials Research Center, Missouri University of Science and Technology, Rolla, MO, USA.
3. DECHEMA, Forschungsinstitut, Frankfurt am Main, Germany
* Corresponding author: chenweit@mst.edu

Metal dusting corrosion is a severe failure mechanism in metallic materials in the petrochemical industry. This form of degradation typically occurs when alloys expose to reducing gaseous environments (CO, H_2, CO_2, H_2O, and CH_4) with and high carbon activity ($a_c > 1$) at a median temperature range (400 – 800°C). Formation of graphite, carbides, and metal dusts on alloys significantly damage the working components. The early establishment of continuous Al_2O_3 scales on the alloy surface can limit graphite nucleation or/and impede inward diffusion of carbon [1,2]. Coupled with this are several recent studies which have shown that susceptibility to metal dusting tends to be much greater under high-pressure exposure conditions [3,4]. Despite the practical importance, studies of metal dusting mechanisms and strategies for improving dusting resistance under pressurized environments are still very limited.

The present work aims to study and compare the microstructures, chemical compositions, and crystallography of oxide scales formed on selected alloys during exposure to controlled dusting conditions at 1 bar and 18 bar. Specifically, we conducted integrated electron beam characterizations on the Ni-based alloy 600 (Ni-17Cr-8Fe) and Fe-based alloy 800H (Fe-31Ni-20Cr) exposed for 250 h at 620°C to 18 bar or 1 bar gas mixtures containing H_2, CO, CO_2, H_2O, and CH_4. The carbon activities at 18 bar and 1 bar were calculated to be 163 and 9, respectively. Pitting was observed on alloy 600 tested at 18 bar (Fig. 1 (a)), while only a limited number of pits were found on the sample exposed at 1 bar (Fig. 1 (b)). Carburization zones comprised of an outer zone of Cr_3C_2 lamellae in an austenitic metal matrix and an internal zone containing the lower chromium carbide, $Cr_{23}C_6$, were observed beneath pits in the 18 bar sample. STEM images (Fig. 3 (a)) and corresponding EDS analysis indicated that the 50 – 150 nm oxide scales consisted of an outer Cr_2O_3 layer and an inner SiO_2+Al_2O_3 layer. Such protective scales were found on the non-attacked surfaces of both samples. Interestingly, ~ 1 nm wide graphite plates were commonly found at Cr_2O_3 grain boundaries near the gas/scale interface in the sample tested at 18 bar (Fig. 3 (b)). No graphite plates were found in the Cr_2O_3 scale formed at 1 bar. The formation of these graphite plates may provide fast paths for inward carbon diffusion and, hence, lead to the onset of metal dusting during exposure to the pressurized environment. This novel observation of graphite plates formed within a thermally grown Cr_2O_3 scale is inferred to be an important aspect of the dusting mechanism at high pressures and will be a topic of further investigation.

Metal dusting corrosion was much more severe on the 800H alloy tested at 18 bar than at 1 bar. Formation of graphite, cementite, iron/chromium oxides, and metal dusts were found in the pitted areas of the 18 bar exposed sample. STEM images (Fig. 4 (a) and (b)) and the corresponding EDS analysis indicated that formation of a continuous Cr_2O_3 scale is the main – albeit finite – protective mechanism for both samples. Consistent with the 600 alloy, graphite plates were only found in the 18 bar sample. Further, a relatively high Fe content (up to 3.2 at%) was found in the Cr_2O_3 scale formed at the 18 bar sample, suggesting that the presence of Fe in the scale may play a role in facilitating graphite nucleation.

References:
[1] DJ Young, *et al*., Materials and Corrosion, **62** (2011), pp. 7-28.
[2] DJ Young, *et al*., JOM, **64** (2012), pp.1461-1469.
[3] S Madloch, *et al*., Oxidation of Metals **89** (2017), pp. 483-498.
[4] M Maier, *et al*., Materials and Corrosion, **49** (1998), pp. 330-335.

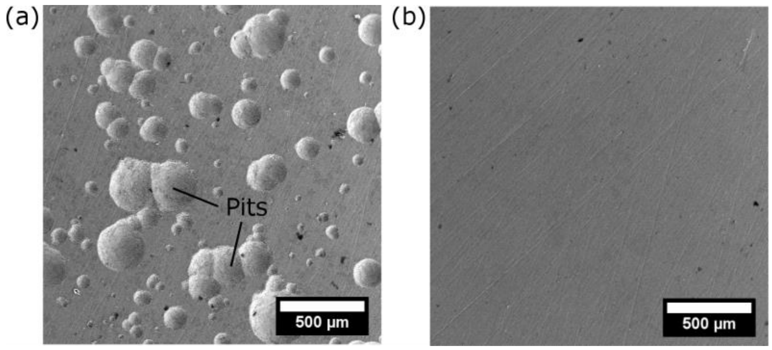

Figure 1. SEM images of the surfaces of the alloy 600 tested at (a) 18 bar and (b) 1 bar at 620°C for 250h

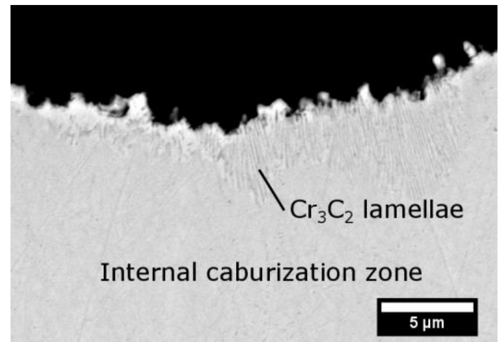

Figure 2. SEM BSE cross-sectional image of pit area in the alloy 600 tested at 18 bar and 620°C for 250h

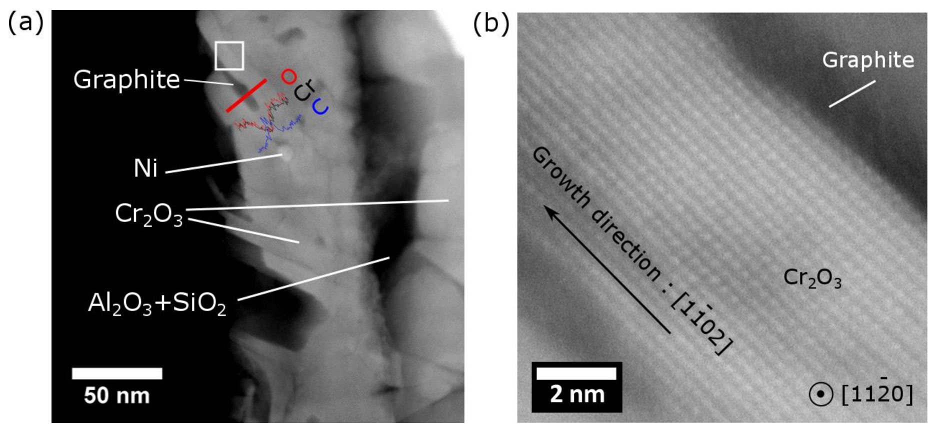

Figure 3. STEM HAADF images of (a) scale on alloy 600 tested at 18 bar with EDS (red line), showing graphite at the Cr_2O_3 boundary, and (b) white box area in (a), showing Cr_2O_3/graphite interface

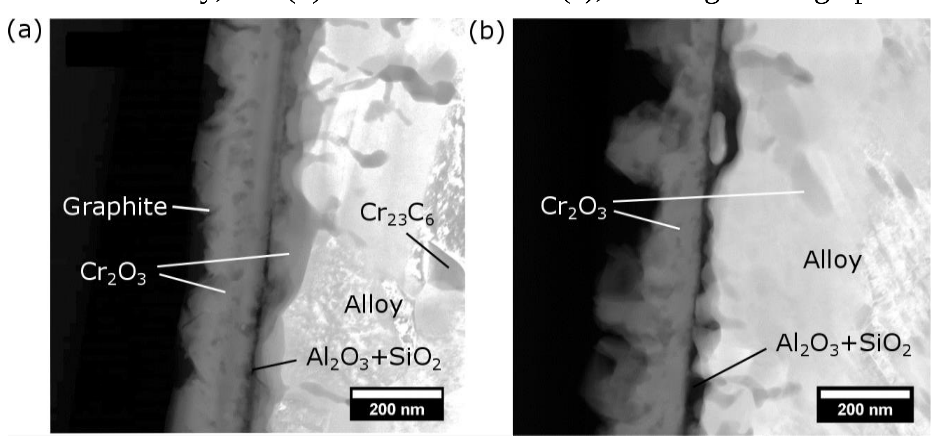

Figure 4. STEM HAADF images of the scales on the alloy 800H tested at (a) 18 and (b) 1 bar at 620°C for 250h

https://doi.org/10.1017/S143192761901239X Published online by Cambridge University Press